IEEE Access
Multidisciplinary ⋮ Rapid Review ⋮ Open Access Journal

Received 5 December 2024, accepted 18 January 2025, date of publication 22 January 2025, date of current version 29 January 2025.

Digital Object Identifier 10.1109/ACCESS.2025.3532787

RESEARCH ARTICLE

A Miniaturized and High Optically Transparent Frequency Selective Surface for RF Shielding Using Double-Glazed Glass Windows for Green Building Applications

MUHAMMAD NASIR[1], SLAWOMIR KOZIEL[1,2], (Fellow, IEEE), AND ADNAN IFTIKHAR[3], (Senior Member, IEEE)

[1]Engineering Optimization and Modeling Center, Reykjavik University, 102 Reykjavík, Iceland
[2]Faculty of Electronics, Telecommunications and Informatics, Gdańsk University of Technology, 80-233 Gdańsk, Poland
[3]Department of Electrical and Computer Engineering, COMSATS University Islamabad, 45550 Islamabad, Pakistan

Corresponding author: Slawomir Koziel (koziel@ru.is)

This work was supported in part by the Icelandic Research Fund under Grant 217771, and in part by the National Science Centre of Poland under Grant 2022/47/B/ST7/00072.

ABSTRACT This research presents a miniaturized and high optically transparent (OT) frequency selective surface (FSS) for achieving RF shielding through glass window panels. The proposed FSS consists of a single-layered copper pattern sandwiched between two ordinary glass substrates to suppress the dual bands of sub-6 fifth generation (5G). In particular, the design effectively shields n65-downlink (2.1 GHz) and a portion of n78-band (3.5 GHz). The unit cell (UC) design consists of square and butterfly rings with a maximum copper width of 0.1 mm. The dimensions of FSS unit cell (UC) are optimized to $0.0714\lambda_0 \times 0.07146\lambda_0$, where λ_0 is the wavelength at 2.1 GHz resonant frequency. Full-wave electromagnetic (EM) simulations, equivalent circuit modeling (ECM), and experimental testing are performed to validate the FSS performance. The design miniaturization and 0.1 mm copper trace width offered a maximum OT of 91.6 % and angular stability up to 85° for both transverse electric (TE) and transverse magnetic (TM) polarized waves.

INDEX TERMS FSS, optical transparency, sub-6 5 GHz, ordinary glass windows, shielding effectiveness.

I. INTRODUCTION

The proliferation of electronic gadgets driven by 5G technology has led to a substantial rise in electromagnetic (EM) radiation levels in both commercial and residential buildings in recent years [1]. Green buildings are a strategic approach to sustainable green development that effectively harnesses ambient energy and light resources. Unwanted EM radiation within these contemporary environmental friendly structures can pose a risk to human well-being and threat to national security [2], [3]. Traditional methods for mitigating and filtering electromagnetic interference (EMI), such as end-to-end encryption and optimization algorithms [4], absorbers, Salisbury screens [5], and common-mode filters [6], have been utilized. Nevertheless, these approaches frequently demonstrate constraints in terms of costs, dimensions, and the capacity to achieve accurate stopbands, as well as an excessive burden on the green infrastructure. Green buildings commonly use FSS's to shield EM radiations. These FSSs are printed directly on the glass windows. The conductive patterns in periodic arrangements can selectively mitigate unwanted EM spectra while still maintaining a high level of transparency for visible light [7]. Historically, FSS has been modeled in array configurations having UC geometry with different patterns to accomplish EM shielding at specific frequency bands, as explained in [8]. The appropriate FSS

The associate editor coordinating the review of this manuscript and approving it for publication was Tanweer Ali.

structures for window glass applications in green buildings simultaneously preserve features such as broad angular stability, strong optical transmission, insensitivity to polarization, and an aesthetically pleasing look. Several methods have been utilized to manufacture these conductive FSS patterns, including screen printing [9], ink-jet printing with silver or nano-inks [10], and additive manufacturing techniques [11], [12]. These methods necessitate the pre-fabrication of the FSS structures on the glass prior to the installation of window glass in the buildings. Furthermore, the non-uniform deposition of conductive ink to draw periodic conductive structures on the glass might lead to imprecise functioning of the FSS.

The fabrication of printed FSS on glass substrates has made significant advancements [13], [14], [15], [16], [17], [18], [19], and [22]. Recently, researchers have created stickers with FSS designs using self-adhesive copper sheets and then applied them to the glass substrate [13]. This technique offered 60° angular stability and achieved a maximum OT of 72% using a conductive strip width of 0.5 mm. In [14], the authors presented a double-glazed glass-based FSS filled with air. This FSS was designed to provide shielding for dual-band WLAN and offered following characteristics: 60° angular stability, a conductor width of 0.4 mm, and an OT of 86 %. Adding a double-sided metallic mesh to the cyclic olefin copolymer (COC) substrate made it much easier for light to pass through by 58.84% [15]. This coating had a conductive strip width of $2\mu m$ and effectively shielded the 5G millimeter-wave band. The integration of a double-layered FSS within a double-glazed glass structure allowed for the simultaneous transmission of signals across a wide range of frequencies used in GSM, while also prevented the interference of undesirable WLAN bands [16]. However, OT of the design is not reported. A newly suggested compact design [17] demonstrated the use of a sandwiched FSS structure positioned between energy-efficient glass layers. This design achieved an OT of 86% with a 0.2 mm-wide copper conductive pattern. Furthermore, it maintained a consistent frequency response of up to 70° for both TE and TM polarizations. By incorporating a transparent dielectric slab onto a glass substrate, the transmission characteristics are improved without negatively affecting OT. Similarly, researchers in [18] created FSS by constructing 0.2 mm conductive loops using copper and silver ink on a polyethylene terephthalate (PTE) substrate, then combined it with a glass substrate to shield the 5G band. The resultant structure demonstrated an OT of 66.6% while simultaneously maintaining angular stability within a range of 30°. The FSS pattern on a double-glazed glass substrate has been reported by [19], to enhance signal transmission, particularly at GSM and WLAN frequencies. In another study [20], a FSS was created on a transparent 0.01 mm thick PET substrate using silver ink with a minimum conductor width of 0.75 mm to achieve maximum visual transparency. Metallic nanomaterial silver ink using a screen-printing approach is employed to produce transparent conformal FSS structures for dual-band EM shielding purposes [21]. The design demonstrated a transparency rate of 81.6% and maintained angular stability of around 70°. A remarkable improvement in OT, reaching 85.3%, was accomplished by utilizing a grid type FSS made with silver (Ag) ink [22]. A dual-layer FSS design [23] effectively shielded the 5G frequency bands ranging from 23.96 to 45.92 GHz, with an impedance bandwidth that exceeds 62.8%.

The literature review indicates that, already reported FSS though offer miniaturized designs but compromise OT and angular stability or vice versa. Also, achieving design compactness by shrinking the width of the metallic strip significantly effects overall shielding effectiveness (SE) of the FSS [24], [25]. The literature review also revealed that the maximum achieved OT is not more than 86% in the FSS design presented so far. In summary, notable dimensions, measured angular stability, and OT values for the double glazed-glass are reported as [$0.12\lambda_0$, 60°, 72%], [$0.16\lambda_0$, 45°, 86%], and [$0.096\lambda_0$, 70°, 86.12%] in [13], [14], and [17], respectively. Therefore, despite notable progress, the achievement of the desired combination of features required for seamless integration of the FSS into double-walled window glass structures, specifically high OT using thin copper patterns, frequency tuning for passive FSS without increasing physical dimensions, and design miniaturization at a low-frequency ratio, are still lacking.

This research aims to address the existing constraints (high OT, compactness, and high angular stability) of the FSS in glass applications by proposing a miniaturized, butterfly shaped sandwiched FSS structure. The proposed structure consists of a single-layered copper conductive pattern sandwiched between two ordinary windows glass substrates. The proposed FSS provides flexibility of the shielded frequency tuning without changing the overall physical dimensions, low-frequency ratio, lower manufacturing cost, and aesthetic look suitable for retrofitting on glass windows for RF shielding. Additionally, the proposed FSS significantly enhances performance features such as OT, wide angular stability, and miniaturization. The symmetrical FSS geometry ensured a strong and identical shielding response for both TE and TM polarizations. In addition, miniaturization has been accomplished by reducing the track width to about 0.1 mm and scaling the dimensions of the FSS to $0.0714\lambda_0 \times 0.0714\lambda_0$. The adopted miniaturization method used to attain high OT than what was previously reported in the literature, as well as a consistent response even at large incident angles for two specific Sub 6–5G frequency bands: n65-downlink (2.1 GHz) and a segment of n78-band (3.5 GHz). In the proposed design, <5 GHz band was deliberately chosen in response to the growing demand for shielding solutions for Sub 6-5G bands. Due to the proliferation of 5G technology, certain restricted sectors, such as hospitals and military facilities, necessitate the shielding of certain frequency bands within their boundaries. Therefore, the proposed solution may serve as a more

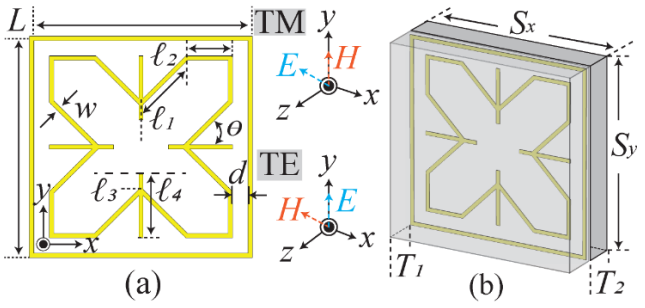

FIGURE 1. Proposed FSS unit cell structure obtained with the help of full-wave simulations: (a) front view, (b) perspective view. The optimized dimensions are $S_x = S_y = 10.4mm$, $L = 10.2mm$, $w = 0.1mm$, $d = 0.91mm$, $\ell_1 = 2.9mm$, $\ell_2 = 2.04mm$, $\ell_3 = 0.75mm$, $\ell_4 = 2.84mm$, and $\theta = 45^\circ$.

realistic solution for such controlled situations to shield the sub-6 5G spectrum.

II. DESIGN AND DEVELOPMENT OF THE FSS UNIT CELL

The proposed UC consists of a sandwiched FSS pattern between two glass substrates with different thicknesses $T_1 =$ 2mm, $T_2 = 1.7$mm, and relative permittivity of $\varepsilon_{r1} = 6.45$ and $\varepsilon_{r2} = 6.15$, respectively [13]. A comprehensive depiction of the precise dimensions and geometrical configuration of the proposed UC is shown in Figure 1. The FSS development began with conventional square loop geometry to attenuate n65 (lower) band. The dimensions are initially estimated using [27]:

$$L \approx c/4f_r \times \sqrt{\varepsilon_{eff}} \tag{1}$$

where c denotes the speed of light, f_r indicates the first resonant frequency, and ε_{eff} represents the effective relative permittivity of the glass substrate. To shield the n78 (higher) band, a butterfly shape was introduced by incorporating 45° symmetric bends at the center point of the inner square loop, along with an additional middle transmission line (TL) called ℓ_4. This centrally located TL modified the electrical length without changing the overall dimensions of the inner butterfly loop.

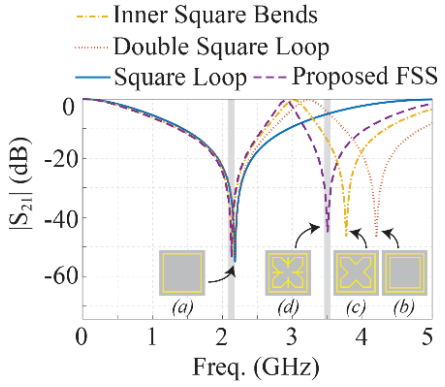

FIGURE 2. Evolution of proposed FSS design and its corresponding simulated transmission coefficient $|S_{21}|$ (dB) graph.

Figure 2 illustrates the process of design evolution and its corresponding frequency responses of each iteration. Each iteration, including the inner square bends, double square loop, and butterfly square loop, demonstrates the steps to reach the final design layout considering the resonances. The proposed FSS UC was simulated and optimized using CST Microwave Studio with Floquet port excitation [28]. As illustrated in Figure 2(a), there is a one transmission zero at 2.18 GHz, which is due to a conventional outer square loop. The second resonance is observed at 4.24 GHz after adding an additional inner square ring, as shown in Figure 2(b). To retain compactness and ensure a stable polarization response, further design modifications were made to shift the second resonance into the n78 band. Specifically, 45° symmetric bends were introduced to the inner square ring, thereby increasing the electrical length without altering the physical size of the UC. This modification resulted in a 3.78 GHz resonance, as shown in Figure 2(c). The final butterfly-shaped structure is illustrated in Figure 2(d), is modeled by incorporating the middle TL (ℓ_4). As a result, the two resonating elements within a UC generating two transmission zeros at 2.1 GHz and 3.5 GHz, with shielding values of 51 dB and 43 dB, respectively. Besides this, a transmission zero was observed at 2.18 GHz due to the presence of a double square ring. However, capacitive coupling between the outer square and the butterfly ring induces a slight shift in the resonance from 2.18GHz to 2.1GHz due to the reduced contact area introduced by the butterfly shape.

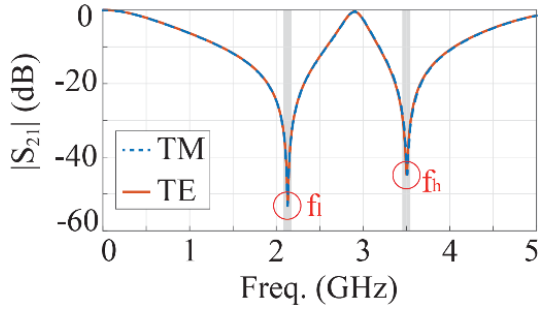

FIGURE 3. Simulated transmission coefficient $|S_{21}|$(dB) response at normal incidence for TE and TM polarization.

In addition, the symmetrical bending in the structure guarantees that the transmission coefficients for both TE and TM polarizations are identical. This is clearly illustrated in Figure 3, which confirms that the design with 90° symmetry offers a polarization-insensitive response. Additionally, Figure 4 illustrates the frequency ratio (FR) plot in relation to variations in θ (where θ is related to symmetrical bending), highlighting the frequency tuning capability of the proposed design. FR defined as the ratio of f_h and f_l, represents the relative spacing between two resonant frequencies. Therefore, f_h/f_l resultant, define specific application's according to variable bands. In the proposed design, FR can be adjusted by varying θ, which is an angle between branch length ℓ_1 and the complete branch length ℓ_4, as depicted in Figure 1 (a).

The variation in ℓ_1 or ℓ_3(a segment of ℓ_4) and relevant placement of ℓ_1 changes θ leading to the longer or shorter electrical lengths for the induced currents. An illustration of the geometrical variations in the butterfly shape in response to pertinent changes of ℓ_1, resulting θ values of 30° and 75°, is depicted in the inset of Figure 4.

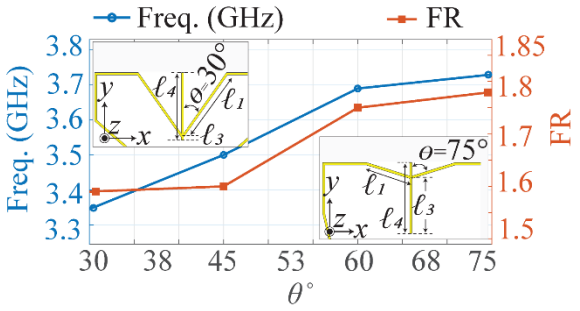

FIGURE 4. Obtained frequency ratio and frequency response at different values of θ.

Note that θ provides flexibility in tuning the frequency without altering the physical dimensions of the FSS. Since θ is directly associated with the butterfly loop, it only provides independent control of n78 resonance band. It can also be observed that higher frequency shielding response (n78) varies from 3.34 GHz to 3.78 GHz, when FR is varied from 1.59 – 1.78. For the final design, θ value of 45° was chosen since it aligns with the intended frequency range i.e., 5G (n78) band. Finally, the compact lattice, and minimum track width of 0.1mm, confirms minimal obstruction of the visual light, thereby facilitating a high OT of 91.6 percent.

III. PERFORMANCE PARAMETERS

A. SURFACE CURRENT DISTRIBUTION ANALYSIS

To predict the FSS shielding characteristics, a current distribution analysis was performed to evaluate the EM behavior and current distribution on the surface of the FSS structure.

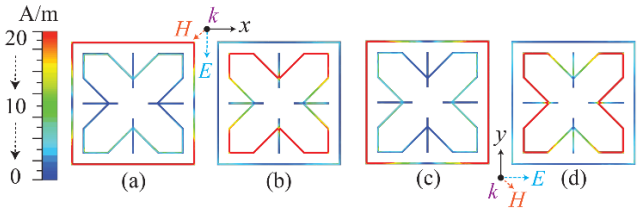

FIGURE 5. Current distribution along the surface of FSS for both polarizations (a). TE polarization at 2.1 GHz (b). TE polarization at 3.5 GHz (c). TM polarization at 2.1 GHz (d). TM polarization at 3.5 GHz.

Figures 5(a) and 5(c) demonstrate that the lowest transmission zero at n65 for both TE and TM polarization is primarily attributed to strong current concentration in the outer square loop. Nevertheless, a less strong current is present around the periphery of the butterfly-shaped structure at n65-band, which is due to the adjacent capacitive coupling.

Conversely, the butterfly-shaped structure undergoes an induction of higher magnitude current only for the purpose of suppressing 3.5 GHz for both TE and TM polarizations. This is illustrated in Figures 5(b) and 5(d). Current distribution analysis also reveals that each section of the FSS generates an independent resonance, enabling individual tuning for respective frequency bands. Also, the current distribution for both TE and TM polarizations exhibits rotational symmetry.

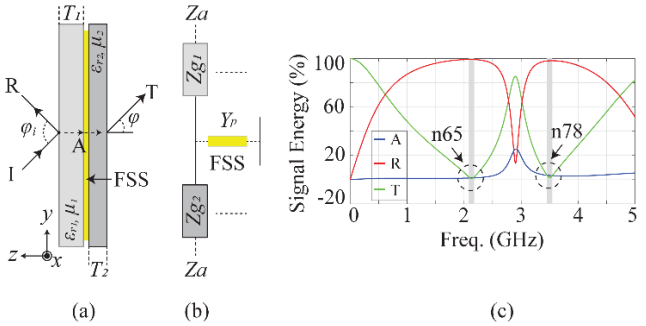

FIGURE 6. Illustration of wave propagation through double layered glass structure (b). equivalent transmission line model, (c). Absorption, transmission, and reflection responses of the proposed FSS structure.

B. SHIELDING MECHANISM

In order to understand the undergoing shielding mechanism of the proposed FSS, the energy distribution of the incoming EM wave on the FSS is analyzed in terms of reflection (R), transmission (T), and absorption (A). For a TE/TM polarized normal incident EM wave, its interaction with the proposed FSS structure sandwiched between two glass substrates is illustrated in Figure 6(a). The absorption phenomena depend on the intrinsic impedances $\left(Zg = Zg_1^{TE/TM}, Zg_2^{TE/TM}\right)$ as it plays an important role in determining the wave propagation characteristics through substrate layers, air impedance ($Z_a = 377\Omega$), and dielectric properties ($\varepsilon_{r1}, \mu_1; \varepsilon_{r2}, \mu_2$) including loss tangent. Additionally, the interaction of the incident wave at a specific incidence angle φ_i and wavelength λ of the wave affects the overall absorption, because change in the incident angle leads to alter wave-impedances of both the TE/TM polarizations [17]. Using 0.01 loss tangent of the glass substrate and conducting pattern's conductivity of $3 \times 10^7 S/m$, the signal energy in terms of reflection, transmission, and absorption of the FSS structure is illustrated in Figure 6(c). The reflection at frequency bands (n65 and n78) are above 90%, whereas the absorption is less than 5%, as shown in Table 1. Therefore, it can be observed from Figure 6 and Table 1 that shielding mechanism of shielding of the proposed design is reflection.

Moreover, an equivalent transmission line model of the proposed FSS configuration is also modeled and a transfer matrix is employed on the wave propagation to predict the transmission coefficient $|S_{21}|$ for the proposed FSS geometry [30]. A representation of the equivalent transmission line model is shown in Figure 6 (b). The intrinsic impedances Z_{g1}, Z_{g2} are modeled as TL, whereas FSS is modelled as a parallel admittance Y_p. The wave propagation through the FSS and the

TABLE 1. Energy distribution through glass substrates for sub6- 5G band.

	N65	N78
Transmission (Co-polarization)	97.92%	94.87%
Reflection (Co-polarization)	0.69%	1.7%
Absorption	1.39%	3.43%
Transmission (Cross-Polarization)	<0.0001%	<0.0001%
Reflection (Co-Polarization)	<0.0001%	<0.0001%

glass layers is modeled using corresponding ABCD parameters, which includes the total transmission matrix, (M_{total}), the effects of the glass layers (M_{glass1} and M_{glass2}) and the FSS (M_{fss}), respectively.

$$M_{total} = M_{glass1} \cdot M_{fss} \cdot M_{glass2} = \begin{pmatrix} A & B \\ C & D \end{pmatrix} \tag{2}$$

$$M_{glass1} = \begin{pmatrix} \cos\left(\beta_{g1} T_{g1}\right) & jZ_g \sin\left(\beta_{g1} T_{g1}\right) \\ j\frac{1}{Z_g} sin\left(\beta_{g1} T_{g1}\right) & \cos\left(\beta_{g1} T_{g1}\right) \end{pmatrix} \tag{3}$$

$$M_{fss} = \begin{pmatrix} 1 & 0 \\ Y_p & 1 \end{pmatrix} \tag{4}$$

$$M_{glass2} = \begin{pmatrix} \cos\left(\beta_{g2} T_{g2}\right) & jZ_g \sin\left(\beta_{g2} T_{g2}\right) \\ j\frac{1}{Z_g} sin\left(\beta_{g2} T_{g2}\right) & \cos\left(\beta_{g2} T_{g2}\right) \end{pmatrix} \tag{5}$$

$$\beta_g = \frac{2\pi n_g}{\lambda_0} \cos\left(\varphi_g\right) \tag{6}$$

$$Z_g = \begin{cases} Z_g{}^{TE} = \frac{Z_a}{\cos(\varphi_g)}; Z_a = 377\Omega \\ Z_g{}^{TM} = Z_a \cos\left(\varphi_g\right) \end{cases} \tag{7}$$

$$M_{glass1} = \delta_1 = \beta_{g1} T_{g1} \tag{8}$$

$$M_{glass2} = \delta_2 = \beta_{g1} T_{g2} \tag{9}$$

$$sin\varphi_g = \frac{sin\varphi_i}{\sqrt{\varepsilon_{r1} + \varepsilon_{r2}}} \tag{10}$$

$$M_1 = M_{glass1} \cdot M_{fss} = \begin{pmatrix} cos\delta_1 + jZ_g \sin\delta_1 \mathrm{Y_p} & jZ_g \sin\delta_1 \\ j * \frac{1}{Z_g} sin\delta_1 & cos\delta_1 \end{pmatrix} \tag{11}$$

$$M_{total} = M_1 \cdot M_{glass2} \tag{12}$$

Equation (2) – (12) represent the transmission matrices, where n_g is the refractive index, φ_g is the refraction angle within the double layered glass substrate, φ_i is the incident angle, and Y_p is the equivalent surface admittance of the FSS pattern. The phase shifts introduced during transmission by the glass substrates are denoted by the terms δ_1 and δ_2. These phase shifts collectively determine the reflection $|S_{11}|$ and transmission $|S_{21}|$ coefficients, which can then be directly related to the absorption calculation ($A = 1 - |S_{11}|^2 - |S_{21}|^2$) to predict the shielding mechanism for an incoming EM wave.

C. POLARIZATION, ANGULAR STABILITY, AND SHIELDING EFFECTIVENESS

1) FSS RESPONSE UNDER TE/TM POLARIZATIONS AND EXTREME INCIDENT ANGLE

The performance of the proposed FSS is evaluated by altering the incident angle of both TE/TM polarized waves from 0°85°. Although, the structure provides similar response under both polarizations due to symmetric nature of design, however, bandwidth diminishes for TE and expands for TM due to the change in the wave impedances [17], [22], which are denoted as; $Z_{TE} = Z_0/\cos(\varphi)$ and $Z_{TM} = Z_0 \cos(\varphi)$,respectively. where Z_0 is the wave impedance 377Ω and φ is the angle of incidence. The FSS filtering response for large incident angles under both polarizations are presented in Figure 7(a) and (b). The results provide unambiguous evidence that the proposed FSS retains excellent angular stability for dual bands under both TE/TM polarized waves. Specifically, the $|S_{21}|$ value remains below −10 dB for incidence angles up to 85°. This wide-angle stable behavior guarantees effective shielding response and practical applicability of the proposed FSS for both sub-6 5G (n65 and n78) bands. Besides this, a slight deviation of around 3% is noticed for 2.1 GHz band at extreme angle for both polarized waves. This can be attributed to the non-uniform surface impedance of the impinging EM waves [29]. However, the offset in resonance remains within the range of frequencies defined by the n65 band.

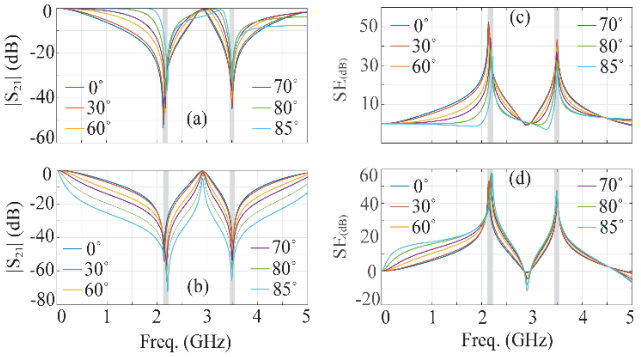

FIGURE 7. Simulated transmission $|S_{21}|$ and shielding effectiveness SE_{dB} response at various incident angles for: (a) and (c). TE-polarization (b) and (d). TM-polarization.

2) SHIELDING EFFECTIVENESS

The resonance behavior dictates how the incident field interacts with the metallic area of the FSS. This is a key factor that affects both frequency selectivity and shielding effectiveness (SE). The FSS's SE is dependent on both the substrate material and metallic properties. Furthermore, the angle at which the incident wave interacts with the FSS surface has an impact on the SE. When TE and TM waves impinge on the FSS structure, absorption and reflection losses exist, which changes the effective path length. This means that the SE can change a lot depending on the angle of incidence. The SE is expressed as:

$$SE\ (dB) = 20 \times \log_{10}\left(\frac{|E_i|}{|E_t|}\right) \tag{13}$$

where E_i and E_t are the linear magnitude of the incident electric field intensity without FSS (considering only glass substrates) and with FSS structure (including glass substrates), respectively, at the designated frequency band.

It should be emphasized that diffraction can directly impact the SE of the FSS. When an incident EM wave impinges on the FSS periodic structure, it can interact with edges and discontinuities, causing diffraction. This can ultimately lead to scattering and wave leakage, thus, potentially reducing SE [35]. However, in the proposed structure, the diffraction effects are mitigated due to periodicity, compact arrangement, and sandwich configuration. This arrangement stabilizes the interaction of the incident EM waves with the FSS and reduces unwanted scattering, ensuring consistent SE across the operating frequency bands.

The SE results of the proposed FSS unit cell are simulated and plotted in Figure 7(c) and (d). According to the results, the SE remains around 50 dB for both TE/TM polarized waves at n65 band as incident angle varies from 0° to 85°. However, when the incident angle reaches maximum value of 85°, the SE for the TE polarized wave decreases steadily to 34. 7 dB within n65 band and to 29dB for n78 band, as depicted in Figure 7(c). Compared with the TM polarized wave, SE gradually increases from 52.40 dB to 57.7 dB at n65 and 43.1 dB to 47.41 dB for n78 band when incidence angle varies from 0° to 85°, as illustrated in Figure 7(d). The observed differences in the SE for TE/TM polarizations are due to changes in reflection, transmission, and absorption because of the corresponding variable wave impedances [29]. However, the steady response of SE is observed at higher incident angle up to 85° for both TE/TM polarizations, which further confirm the minimal impact of diffraction, making the design robust for double glazed glass-based applications.

D. OPTICAL TRANSPARENCY

In order to assess the suitability of the proposed FSS for RF shielding in the green buildings, it is imperative that the FSS structure does not have any impact on the amount of daylight entering the building. The feature of the FSS is defined by optical transparency (OT). The OT at visible light is dictated by the combined area of the conductive pattern in the FSS structure and the transparent substrate.

Typically, transparent ink-based conductive patterns are employed on the glass substrate to obtain high OT. However, these methods encounter manufacturing limitations and non-uniform deposition of ink may affect SE. In addition, increasing the periodicity of the FSS structure can also enhance OT, but this comes with drawbacks of significant side effects, including deterioration in the incident angle's stability. Hence, FSS geometry must provide excellent shielding performance and high OT for RF shielding applications in green buildings. Therefore, OT of the proposed FSS is computed analytically using the fact that glass as a substrate is the transparent portion, whereas the thin copper patterns that are on the top of the glass substrate are opaque. The OT is defined as the ratio of total conductive area of the unit cell to the total area of the glass substrate. Mathematically, the OT (η) is expressed as,

$$\eta\,(\%) = \left(1 - \frac{A_m}{A_s}\right) \times 100 \tag{14}$$

where A_m and A_s represent, the total metallic area of the FSS unit cell and the total substrate area, respectively. Using 0.1 mm thin conductive strips resulted in a total conductive area of 9.04 mm^2, while the substrate encompassed 108.16 mm^2 area, resulting in OT of approximately 91.6%.

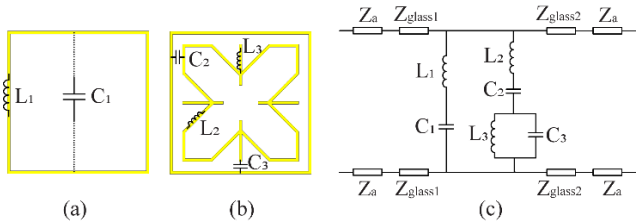

FIGURE 8. Mapping of the lumped elements on the proposed FSS structure at resonator (a) outer square loop and (b). inner butterfly ring. (c). Finalized equivalent circuit model of the proposed FSS. Optimized values of inductors and capacitors are $L_1 = 9.45nH$, $C_1 = 0.59pF$, $L_2 = 6.8nH$, $C_2 = 0.2pF$, $L_3 = 2.75nH$, and $C_3 = 0.16pF$.

IV. EQUIVALENT CIRCUIT MODEL

To elucidate the underlying physical mechanism of the FSS unit cell and provide a simplified representation of the complex EM behavior, a representation of associated LC elements to each resonator and lumped element-based equivalent circuit is modeled. A detailed mapping of the lumped element is illustrated in Figure 8(a) and (b) against each resonator, and its simplified corresponding equivalent circuit model from the LC mapping is illustrated in Figure 8(c). The outer square ring resonator is modeled as an inductor L_1, while net capacitance C_1 encounters the coupling between each adjacent unit cells [31]. The inductor L_2 corresponds to the inner bent square resonator, whereas C_2 represents coupling between the inner butterfly ring and the outer square loop. Inductor L_3 corresponds to the additional length of the middle TL and capacitance C_3 relates the adjacent coupling effects. The glass substrates having variable thicknesses are modeled as TLs and their corresponding impedances are calculated using:

$$Z_{glass1} = Z_{glass2} = Z_a / \sqrt{\varepsilon_r} \tag{15}$$

where Z_a is the impedance of free space i.e., 377Ω. It can be observed from Figure 8(c), that the inductors (L_1, L_2, L_3) and capacitive (C_1, C_2, C_3) of each resonator are in parallel configuration and surface impedances of each resonator in the proposed FSS design are independent. Z_{fss1} represents the total surface impedance of the outer square ring, whereas the butterfly ring resonator's total surface impedance is represented by Z_{fss2}. These surface impedances are calculated as follows [32]:

$$Z_{fss1} = \frac{1 - \omega^2 L_1 C_1}{j\omega C_1} \tag{16}$$

And,

$$Z_{fss2} = \frac{1 - \omega^2 L_2 C_2}{j\omega C_2} + \frac{j\omega L_3}{1 - \omega^2 L_3 C_3}. \tag{17}$$

The transmission zeros at both bands for both resonant elements are extracted by equating the numerators of (16) and (17) to zero.

$$f_{n65} = \frac{1}{2\pi}\sqrt{\frac{1}{L_1C_1}} \tag{18}$$

And,

$$f_{n78} = \frac{1}{2\pi}\sqrt{\frac{L_2C_2 + L_3C_3 + L_3C_2 - x}{2L_3C_3L_2C_2}}$$

$$x = \sqrt{(L_2C_2 + L_3C_3 + L_3C_2)^2 - 4(L_3C_3L_2C_2)} \tag{19}$$

First the transmission zeros at 2.1 GHz and 3.5 GHz are calculated using (18) and (19), respectively, after extracting the optimized values of inductors and capacitors using Keysight ADS. The ECM results illustrate good agreement with the full wave EM results, as shown in Figure 9.

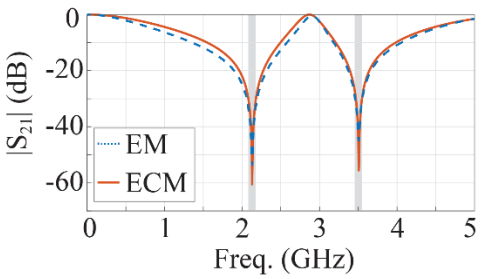

FIGURE 9. A comparison of the transmission characteristics of the proposed FSS between EM simulation and circuit model.

V. EXPERIMENTAL VALIDATION

The proposed FSS was experimentally evaluated to verify the accuracy of the simulation findings and assess the practical efficiency of the design. A prototype of a finite array with dimensions of $260 \times 176.8\, mm^2$, containing 17×25-unit cells was fabricated on the commercially available glass substrates. In the fabrication method, conductive patterns of the finite FSS array are etched on $35\mu m$ thick self-adhesive copper sheets (shown in Figure 10(a)) using a chemical etching process. The prepared FSS array, created a sticker, is accurately applied onto a 1.7 mm thick glass substrate. Another 2 mm thick glass substrate is then adhered to create a sandwich structure to depict double glass windows model. A photograph of the fabricated prototype is shown in Figure 10(b). The use of low-cost self-adhesive copper sheets in the fabrication process of the prototype overcomes the challenges posed by expensive additive manufacturing technologies. Furthermore, it resolves issues related to application size, uneven conductive layer thickness, and the conductivity of silver inks. This method also avoids the prefabrication of the FSS structure before the installation of glass windows in green buildings.

Following the fabrication, the prototype underwent experimental testing using the free-space measurement method. The measurement setup is shown in Figure 10(c). The prototype was fixed in the aperture of an aluminum sheet having

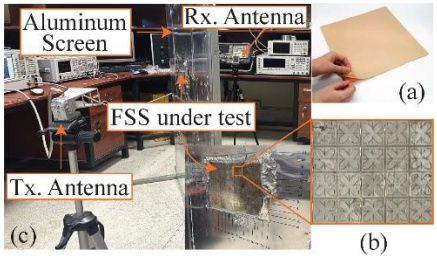

FIGURE 10. (a) Photograph of self-adhesive copper sheet used as a conductor. (b) Magnified view of the fabricated prototype. (c) measurement setup adopted for experimental verification of the FSS prototype.

size of $10\boldsymbol{\lambda_0}$ to ensure that impinging EM waves from the transmitting antenna are only passing through the prototype placed in the aperture. A pair of horn antennas (model # LB-20265) [33] connected to a calibrated network analyzer (model # N5242A) were used as transmitter and receiver with a distance of 2 meters to ensure far-field conditions. Free space calibrations were performed initially and then prototype was placed in the aperture to record $|S_{21}|$ values to validate shielding responses at various incident angles for TE/TM polarized waves. Figure 11 depicts comparison between measured (*dashed lines*) and simulated (*solid lines*) shielding responses for both the TE and TM polarized waves. Owing to symmetrical structure, both TE and TM polarized waves produced adequate suppression around 40 – 60 dB at both n65 and n78 bands, respectively. It can be observed in Figure 11(a) and (b) that the measured shielding response for the TE polarized wave is around 60 dB at a 0° incident angle which decrease shown to 40 dB at 70°. Notably, at an extreme angle of 70°, a -10 dB bandwidth of 1.75 GHz is observed at the n78 band which is attributed to the change in wave impedance. Despite this, the shielding response remains consistent across both the bands for the incident angles ranging from 0° to 85°. Similarly, measured shielding responses for the TM polarized wave agree well with the simulated results, as shown in Figure 11(c) and (d). Additionally, there exists a slight shift in the resonance at both the bands when incidence angle reaches 85°. This slight shift results in frequency error ratio of around 1.5% for TE and 4% for TM polarized wave. Overall, a minor disagreement between simulated and measured shielding response is attributed to the finite FSS array size, measurement imperfections, and fabrication tolerances. Notably, it can be observed from the measured results that at 85° incident angles, there exist significant disagreement with the simulated results. Because the aluminum sheet is rotated at 85°, there is a noticeable misalignment between the horn antennas. At higher angles, such as 85°, increased multiple EM reflections do not ensure EM wave transmissions on the FSS sheet, which distorted the results significantly and introduced measurements imperfections at 85° [17].

VI. COMPARISON

Finally, the proposed FSS design was compared with the existing FSS designs that are fabricated using copper and

TABLE 2. Comparison of the proposed FSS with the existing fss designs in literature.

Ref.	UCS	FB (GHz)	AS (TE/TM)	MT (η)	No. of (S/MS) layers	Types of CM	Max. TW (mm)
[13]	$0.12\lambda_0$	1.8 / 2.5 / 5.6	60°	72%	2/1	Copper	0.5
[14]	$0.16\lambda_0$	2.45 / 5.5	45°	86%	2/1	Copper	0.4
[15]	$0.224\lambda_0$	28	50°	58.84%	2/1	Copper	0.2
[16]	$0.245\lambda_0$	2.45 / 5.34	60°	NR	2/2	Aluminum	3
[17]	$0.096\lambda_0$	2.45 / 3.5	70°	86.12%	2/1	Copper (Silver finish)	0.2
[18]	$0.22\lambda_0$	28	30°	66.6%	2/1	Copper	0.25
[20]	$0.083\lambda_0$	2	60°	NR	1/1	Silver Ink	0.75
[21]	$0.18\lambda_0$	0.98 / 1.95	TM = 0° − 60° TE = 0° − 70°	81.6%	1/1	Silver (nanowire) (Ag NW)	0.05
[26]	$0.0807\lambda_0$	0.9 / 2.6 / 5.7	60°	NR	1/2	Copper (Silver finish)	1.84
This work	$\mathbf{0.0714\lambda_0}$	**2.1 / 3.5**	**85°**	**91.6%**	**2/1**	**Copper**	**0.1**

***UCS:** Unit cell size, **FB:** Frequency bands, **AS:** Angular Stability, **MT:** Maximum Transparency, **S/MS:** Substrate/ Meta surfaces, **CM:** Conductive material, **FR:** Frequency ratio, **NR:** Not Reported, **TW:** Track Width

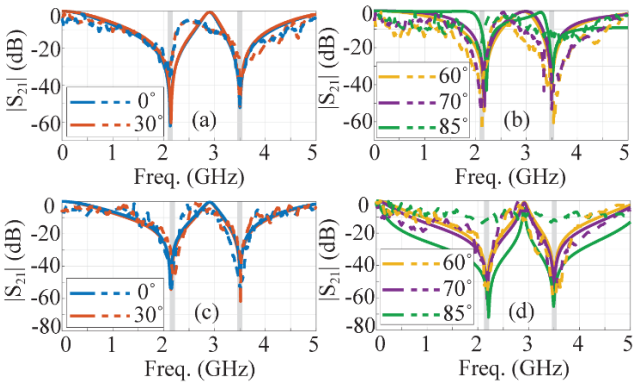

FIGURE 11. Comparison between simulated and measured results of the proposed FSS at different incident angles for (a) TE and (b) TM polarized waves.

conductive inks for achieving RF shielding through glass windows. A detailed comparison is tabulated in Table 2. The comparison provides a concise overview of the key parameters including dimensions, angular stability, and maximum transparency offered by the proposed FSS. The proposed FSS design incorporates smaller dimensions and thin copper tracks, which are essential for achieving maximum transparency. As observed in Table 2, designs reported in [20] and [21] utilized AgNW inks instead of copper as a conductive material. In comparison, the proposed FSS provides a cost-effective alternative by employing self-adhesive copper sheets in place of AgNW inks, thus alleviating the limitations associated with AgNW. AgNW inks are generally more expensive and less suitable for large-scale manufacturing of periodic structures because of their elevated surface roughness and inconsistent thickness. Furthermore, FSS array is a sandwiched configuration, which does not only protect the copper from environmental exposure but also ensures long-term stability and endurance. Additionally, associated problems with AgNWs, including poor adhesion, susceptibility to de-lamination from the substrate, and uneven thickness, making the use of AgNW's less practical for the glass-based applications [34].

It can also be observed from Table 2 that [26] proposes a triple-band butterfly type design for energy harvesting application, offering high efficiency and a single layer structure. This butterfly design incorporates 1.84 mm thick trace width and two through-hole via's are inserted in its geometry for energy harvesting. In contrast, the proposed FSS is geometrically a combination of square and butterfly type design that has trace width of 0.1 mm. Also, its distinct shapes provide robust control to tune the shielded frequency, whereas [26] lacks this feature. In addition, the proposed design has notable contributions in terms of OT which is 91.6 % and up to 85° angular stability. Finally, a simpler fabrication process adopted effectively eliminates fabrication complexity due to via's [26] and ultimately enhances practical aspect of such designs in realizing periodic structures.

In summary, it can be argued that the proposed FSS demonstrates enhanced miniaturization, wide-angle angular stability, and high OT, as compared to relevant designs encapsulated in Table 2. Also, the proposed design is suitable for practical applications for achieving RF shielding through glass windows and their easy installation in green buildings. Compared to the existing designs, the proposed FSS has a compact trace width of 0.1 mm which translates into a maximum OT of 91.6%, outperforming other designs and providing a reliable RF shielding solution for green buildings without affecting daylight. The proposed FSS also offers advancements compared to [17], such as high OT (91.6% vs. 86.12%), higher angular stability (85° vs. 70°), and compact

unit cell size ($0.0714\lambda_0 \times 0.0714\lambda_0$ vs. $0.096\ \lambda_0 \times 0.096\ \lambda_0$), which corresponds to about 29.39% size reduction. Additionally, in [17], the relative shielding bandwidth decreases down to 29.8 % at 3.5 GHz frequency when incidence angle is 80°. On the other hand, the proposed design offers 45.57 % shielded bandwidth at 3.5 GHz. Besides this, the fabrication process in [17] involves initial copper deposition followed by etching. Whereas the proposed FSS utilizes a cost-effective retrofitting fabrication method, employing self-adhesive copper sheets. The retrofitting approach streamlines the practical application of this design, enabling users to install the FSS structure on any existing glass windows which enhances the practicality of the proposed structure.

VII. CONCLUSION

This research showcased the development of a highly OT FSS suitable for RF shielding through glass windows installed in green buildings. The proposed FSS structure offers excellent effective shielding at two sub-6 5G bands (n65 and n78) while maintaining OT of 91.6 % using maximum copper trace width of 0.1 mm. In addition, the SE remains intact for TE and TM polarized EM waves with incidence angle variations up-to 85°. The experimental testing validated the SE exceeding 29 dB and 47dB for both bands having wide-angle angular stability under TE/TM polarized waves. With its design compactness, frequency tuning option, and utilization of self-adhesive copper sheets in design fabrication, the proposed FSS offers great promise for seamlessly achieving RF shielding in contemporary building architectures while maintaining both aesthetic appeal and functionality.

ACKNOWLEDGMENT

The authors would like to thank Dassault Systèmes, France, for making CST Microwave Studio available.

REFERENCES

[1] H. Yang, L. Chen, H. Liu, and G. Zhu, "Dynamic feature-fused localization with smartphones exploiting 5G NR SSB and Wi-Fi for indoor environments," *IEEE Trans. Instrum. Meas.*, vol. 73, pp. 1–14, 2024.

[2] P. Testolina, M. Polese, J. M. Jornet, T. Melodia, and M. Zorzi, "Modeling interference for the coexistence of 6G networks and passive sensing systems," *IEEE Trans. Wireless Commun.*, vol. 23, no. 8, pp. 9220–9234, Aug. 2024.

[3] A. A. Salas-Sánchez, A. López-Furelos, J. A. Rodríguez-González, F. J. Ares-Pena, and M. E. López-Martín, "Validation of potential effects on human health of in vivo experimental models studied in rats exposed to sub-thermal radiofrequency. Possible health risks due to the interaction of electromagnetic pollution and environmental particles," *IEEE Access*, vol. 7, pp. 79186–79198, 2019.

[4] R. Gallego-Martínez, F. J. Muñoz-Gutiérrez, and A. Rodríguez-Gómez, "Trajectory optimization for exposure to minimal electromagnetic pollution using genetic algorithms approach: A case study," *Exp. Syst. Appl.*, vol. 207, Nov. 2022, Art. no. 118088.

[5] S. Geetha, K. K. S. Kumar, C. R. K. Rao, M. Vijayan, and D. C. Trivedi, "EMI shielding: Methods and materials—A review," *J. Appl. Polym. Sci.*, vol. 112, no. 4, pp. 2073–2086, Feb. 2009.

[6] J. Liu, Y. Zhang, D. Jiang, X. Zhao, and Z. Liu, "Insertion loss analysis and optimization of a current based common-mode active EMI filter," *IEEE Trans. Power Electron.*, vol. 39, no. 11, pp. 14353–14362, Nov. 2024.

[7] T. Chaloun, S. Brandl, N. Ambrosius, K. Kröhnert, H. Maune, and C. Waldschmidt, "RF glass technology is going mainstream: Review and future applications," *IEEE J. Microw.*, vol. 3, no. 2, pp. 783–799, Apr. 2023.

[8] B. Munk, *Frequency Selective Surfaces, Theory and Design*. New York, NY, USA: Wiley, 2000.

[9] D. J. King, K. Hettak, M. R. Chaharmir, and S. Gupta, "Flexible ink-minimized screen-printed frequency selective surfaces with increased optical transparency for 5G electromagnetic interference mitigation," *IEEE Trans. Compon., Packag., Manuf. Technol.*, vol. 13, no. 1, pp. 110–119, Jan. 2023.

[10] J. Zhou, S. Yu, and N. Kou, "A frequency selective rasorber with absorption bands on both sides of passband based on screen-printed resistive film," *IEEE Antennas Wireless Propag. Lett.*, vol. 23, no. 11, pp. 3912–3916, Nov. 2024.

[11] A. Shastri, B. Sanz-Izquierdo, A. Elibiary, and E. A. Parker, "Manufacturing, developments, and constraints in full 3-D printing of frequency-selective surface using low-cost open-source printer," *IEEE Trans. Compon., Packag., Manuf. Technol.*, vol. 11, no. 12, pp. 2193–2200, Dec. 2021.

[12] S. Ghosh and S. Lim, "A miniaturized bandpass frequency selective surface exploiting three-dimensional printing technique," *IEEE Antennas Wireless Propag. Lett.*, vol. 18, no. 7, pp. 1322–1326, Jul. 2019.

[13] U. Farooq, M. F. Shafique, A. Iftikhar, and M. J. Mughal, "Polarization-insensitive triband FSS for RF shielding at normal and higher temperatures by retrofitting on ordinary glass windows," *IEEE Trans. Antennas Propag.*, vol. 71, no. 4, pp. 3164–3171, Apr. 2023.

[14] U. Farooq, M. F. Shafique, and M. J. Mughal, "Polarization insensitive dual band frequency selective surface for RF shielding through glass windows," *IEEE Trans. Electromagn. Compat.*, vol. 62, no. 1, pp. 93–100, Feb. 2020.

[15] H. Chen, H. Chen, X. Xiu, Q. Xue, and W. Che, "Transparent FSS on glass window for signal selection of 5G millimeter-wave communication," *IEEE Antennas Wireless Propag. Lett.*, vol. 20, no. 12, pp. 2319–2323, Dec. 2021.

[16] F. Bagci, C. Mulazimoglu, S. Can, E. Karakaya, A. E. Yilmaz, and B. Akaoglu, "A glass based dual band frequency selective surface for protecting systems against WLAN signals," *AEU-Int. J. Electron. Commun.*, vol. 82, pp. 426–434, Dec. 2017.

[17] Z. Chen, Y. Li, Z. Wang, J. Hu, and X. Yao, "Energy-saving glass loading dual-band miniaturized FSS for RF shielding with high oblique stability and optical transparency," *IEEE Trans. Electromagn. Compat.*, vol. 66, no. 4, pp. 1094–1103, Aug. 2024.

[18] D. T. Nguyen, J.-N. Lee, J. I. Moon, and C. W. Jung, "Single-layer frequency-selective surface on window glass for 5G indoor communications," *IEEE Antennas Wireless Propag. Lett.*, vol. 23, no. 5, pp. 1558–1562, May 2024.

[19] S. I. Sohail, K. P. Esselle, and G. Kiani, "Design of a bandpass FSS on dual layer energy saving glass for improved RF communication in modern buildings," in *Proc. IEEE Int. Symp. Antennas Propag.*, Chicago, IL, USA, Jul. 2012, pp. 1–2.

[20] A. A. Dewani, S. G. O'Keefe, D. V. Thiel, and A. Galehdar, "Window RF shielding film using printed FSS," *IEEE Trans. Antennas Propag.*, vol. 66, no. 2, pp. 790–796, Feb. 2018.

[21] Y. Yang, W. Li, K. N. Salama, and A. Shamim, "Polarization insensitive and transparent frequency selective surface for dual band GSM shielding," *IEEE Trans. Antennas Propag.*, vol. 69, no. 5, pp. 2779–2789, May 2021.

[22] R. Z. Jiang, Q. Ma, J. C. Liang, Q. Y. Zhou, J. Y. Dai, Q. Cheng, and T. J. Cui, "A single-layered wideband and wide-angle transparent metasurface for enhancing the EM-wave transmissions through glass," *IEEE Trans. Antennas Propag.*, vol. 71, no. 8, pp. 6593–6605, Aug. 2023.

[23] M. L. Hakim, M. T. Islam, and T. Alam, "Incident angle stable broadband conformal mm-wave FSS for 5G (n257, n258, n260, and n261) band EMI shielding application," *IEEE Antennas Wireless Propag. Lett.*, vol. 23, no. 2, pp. 488–492, Feb. 2024.

[24] S. Dey and S. Dey, "Conformal multifunction FSS with enhanced capacitance loading for high angle stable stopband filtering and microwave absorption," *IEEE Trans. Electromagn. Compat.*, vol. 64, no. 2, pp. 315–326, Apr. 2022.

[25] M. L. Hakim, T. Alam, and M. T. Islam, "Polarization insensitive and oblique incident angle stable miniaturized conformal FSS for 28/38 GHz mm-wave band 5G EMI shielding applications," *IEEE Antennas Wireless Propag. Lett.*, vol. 22, no. 11, pp. 2644–2648, Nov. 2023.

[26] X. Zhang, H. Liu, and L. Li, "Tri-band miniaturized wide-angle and polarization-insensitive metasurface for ambient energy harvesting," *Appl. Phys. Lett.*, vol. 111, no. 7, Aug. 2017, Art. no. 071902.

[27] S. Habib, G. I. Kiani, and M. F. U. Butt, "A convoluted frequency selective surface for wideband communication applications," *IEEE Access*, vol. 7, pp. 65075–65082, 2019.
[28] Dassault Systemes. *CST-Computer Simulation Technology Microwave Studio Suite*. Accessed: Nov. 10, 2024. [Online]. Available: https://www.cst.com
[29] A. Araghi, M. Khalily, M. Safaei, A. Bagheri, V. Singh, F. Wang, and R. Tafazolli, "Reconfigurable intelligent surface (RIS) in the sub-6 GHz band: Design, implementation, and real-world demonstration," *IEEE Access*, vol. 10, pp. 2646–2655, 2022.
[30] D. M. Pozar, *Microwave Engineering*. New York, NY, USA: Wiley, 2012.
[31] M. A. Rodriguez Barrera and W. P. Carpes, "Bandwidth for the equivalent circuit model in square-loop frequency selective surfaces," *IEEE Trans. Antennas Propag.*, vol. 65, no. 11, pp. 5932–5939, Nov. 2017.
[32] S. Ghosh and K. V. Srivastava, "An equivalent circuit model of FSS-based metamaterial absorber using coupled line theory," *IEEE Antennas Wireless Propag. Lett.*, vol. 14, pp. 511–514, 2015.
[33] *Horn Antenna*. Accessed: Nov. 10, 2024. [Online]. Available: https://www.ainfostore.com/lb-20265-sf-broadband-horn-antenna-2-26-5-ghz-13db-gain-sma-female
[34] M. Azani, A. Hassanpour, and T. Torres, "Benefits, problems, and solutions of silver nanowire transparent conductive electrodes in indium tin oxide (ITO)-free flexible solar cells," *Adv. Energy Mater.*, vol. 10, no. 48, Dec. 2020, Art. no. 2002536.
[35] C. Balanis, *Advanced Engineering Electromagnetics*. Hoboken, NJ, USA: Wiley, 2012, ch. 13.

MUHAMMAD NASIR received the B.S. and M.S. degrees in electrical engineering from COMSATS University Islamabad (CUI), Pakistan, in 2015 and 2020, respectively. He is currently pursuing the Ph.D. degree with the Department of Engineering, Reykjavik University, Iceland. His research interests include multilayer antennas array and metasurfaces.

SLAWOMIR KOZIEL (Fellow, IEEE) received the M.Sc. and Ph.D. degrees in electronic engineering from Gdańsk University of Technology, Poland, in 1995 and 2000, respectively, the M.Sc. degree in theoretical physics, in 2000, the M.Sc. degree in mathematics, in 2002, and the Ph.D. degree in mathematics from the University of Gdańsk, Poland, in 2003. He is currently a Professor with the Department of Engineering, Reykjavik University, Iceland. His research interests include CAD and modeling of microwave and antenna structures, simulation-driven design, surrogate-based optimization, space mapping, circuit theory, analog signal processing, evolutionary computation, and numerical analysis.

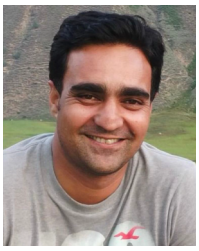

ADNAN IFTIKHAR (Senior Member, IEEE) received the B.S. degree in electrical engineering (telecommunication) from COMSATS University Islamabad (CUI), Islamabad, Pakistan, in 2008, the M.S. degree in personal mobile and satellite communication from the University of Bradford, Bradford, U.K., in 2010, and the Ph.D. degree in electrical and computer engineering from North Dakota State University (NDSU), Fargo, ND, USA, in 2016. He is currently an Assistant Professor with the Department of Electrical Engineering, CUI, and on a post-doctoral study leave. He is also a Marie Skłodowska-Curie Fellow and a Research Executive with Hacettepe University, Ankara, Türkiye, where he is researching on flexible substrate for antenna designing in biomedical and wearable applications. He has authored or co-authored 85 journals and conference publications. He was a recipient of various national and international funding. He has established various RF research facilities with CUI. His research interests include reflectarray antennas, multilayer antennas, wearable biomedical antennas, frequency selective surfaces, and metamaterial absorbers. He has been actively engaged as a reviewer of RF and antenna related international journals.